ACS APPLIED MATERIALS & INTERFACES

www.acsami.org

Research Article

Two-Photon Polymerization of Butterfly Wing Scale Inspired Surfaces with Anisotropic Wettability

Zefu Ren,[‖] Zhuoyuan Yang,[‖] Rishikesh Srinivasaraghavan Govindarajan, Foram Madiyar, Meng Cheng,* Daewon Kim,* and Yizhou Jiang*

Cite This: *ACS Appl. Mater. Interfaces* 2024, 16, 9362−9370

Read Online

ACCESS | Metrics & More | Article Recommendations | Supporting Information

ABSTRACT: Wings of Morph aega butterflies are natural surfaces that exhibit anisotropic liquid wettability. The direction-dependent arrangement of the wing scales creates orientation-turnable microstructures with two distinct contact modes for liquid droplets. Enabled by recent developments in additive manufacturing, such natural surface designs coupled with hydrophobicity play a crucial role in applications such as self-cleaning, anti-icing, and fluidic manipulation. However, the interplay among resolution, architecture, and performance of bioinspired structures is barely achieved. Herein, inspired by the wing scales of the Morpho aega butterfly, full-scale synthetic surfaces with anisotropic wettability fabricated by two-photon polymerization are reported. The quality of the artificial butterfly scale is improved by optimizing the laser scanning strategy and the objective lens movement path. The corresponding contact angles of water on the fabricated architecture with various design parameters are measured, and the anisotropic fluidic wettability is investigated. Results demonstrate that tuning the geometrical parameters and spatial arrangement of the artificial wing scales enables anisotropic behaviors of the droplet's motion. The measured results also indicate a reverse phenomenon of the fabricated surfaces in contrast to their natural counterparts, possibly attributed to the significant difference in equilibrium wettability between the fabricated microstructures and the natural Morpho aega surface. These findings are utilized to design next-generation fluid-controllable interfaces for manipulating liquid mobility on synthetic surfaces.

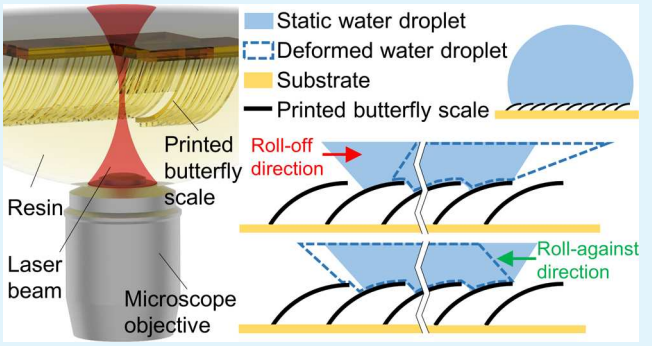

KEYWORDS: *butterfly wing scale, bioinspired microstructures, two-photon polymerization, anisotropic wettability, additive manufacturing*

1. INTRODUCTION

Natural structures found in organisms have evolved over thousands of years to be functionally efficient. Such structures in biosystems can exhibit various properties, including high strength-to-mass ratio, adhesion, fluid direction controllability, and hydrophobicity.[1−6] Particularly, hydrophobic surfaces exist naturally in plants and insects like lotus leaves, rice leaves, beetle elytra, and butterfly wings.[7−9] These structures hold great promise for applications in modern engineering and the manufacturing sector. Inspired by natural hydrophobic surfaces, artificial surfaces often exhibit macro- to nanoscale hierarchical structures comprising a range of features organized in a structured geometric pattern. The integrated structure composed of ordered features provides the means to manipulate the interfaces and dynamics of liquid−air and liquid−solid interactions. Consequently, the presence of hierarchical microstructures and nanostructures can improve hydrophobicity by promoting a high contact angle of water.[10]

With the recent development in additive manufacturing (AM), the fabrication of bioinspired hydrophobic structures is enabled.[10−12] Many AM techniques, including fused deposition modeling (FDM), selective laser melting (SLM), and digital light processing (DLP), have been used to rapidly prototype and develop such hydrophobic surfaces. Among them, FDM is an extrusion-based AM method using polymer-based filaments. The filament is melted by passing through a heated nozzle and deposited on a heated platform when the filament is in the semiliquid state. The resolution of the printed part produced by common FDM is approximately 0.1 mm.[13] While FDM is widely recognized as a cost-effective three-dimensional (3D) printing method, its capability to fabricate small-scale bioinspired features is relatively limited due to its sub-par resolution in microscale manufacturing.[14] Alternatively, SLM is a powder-based AM technique, which fuses the uniformly spread metallic powder with a high-power laser to

Received: October 3, 2023
Revised: January 17, 2024
Accepted: January 22, 2024
Published: February 7, 2024

produce the metallic structure layer by layer.[15] It enables the fabrication of metallic bioinspired hydrophobic structures with high strength, enhanced impact resistance, and high thermal conductivity.[16] For instance, Mekhiel et al. showcased a bioinspired structure printability utilizing partially fused stainless steel microparticles to achieve hydrophobicity on a 3D-printed metal structure.[17] However, the resolution of SLM products is based on the laser beam spot size, which is typically about 70 to 200 μm.[15] The spatial arrangement of hierarchical features may suffer from some imprecision and inconsistency due to irregular particle size and thermal cycling. Conversely, DLP is a projection-based AM technique utilizing liquid photosensitive resin, which is selectively cured by controlled ultraviolet (UV) light exposure to print a 3D structure in a layer-by-layer formation. It is capable of producing polymer-based bioinspired structures with a resolution ranging from 15 to 100 μm.[18] Davoudinejad et al. fabricated gecko-inspired adhesive surfaces, featuring two- or three-leveled hierarchical micropillars, via UV polymerization, demonstrating high contact angle of water.[19] However, the printed feature using DLP tends to be significantly larger than its natural counterparts, and achieving complex geometries can be challenging.

Hence, the pursuit of a reliable method to accurately fabricate 3D microstructures has become imperative. Two-photon polymerization (TPP) emerges as a promising submicroscale AM technique, where a small spatial region within the liquid photosensitive resin is polymerized when two photons are simultaneously absorbed by activating lasers.[20] The polymerization process is initiated when the absorbed energy of the photosensitive resin surpasses a specific threshold. The photosensitive material around the center of the laser's focal point is solidified to form an ellipsoidal particle, namely, a voxel, because of the cross-linking of the polymer chains.[21] The diameter of the voxel gradually diminishes vertically, forming a parabolic shape due to the nonlinear reduction in energy intensity away from the focal point, eventually dropping below the polymerization energy threshold. As a result, the printed structures consist of periodically arranged voxels based on the laser scanning path according to the programmed digital file. Additionally, the voxel size depends on factors such as the type of objective lens as well as the optimal combination of laser scanning speed and power. Both horizontally and vertically, multiple neighboring voxels overlap with optimal hatching and slicing distances to form a stable structure. The superior resolution of TPP enables the fabrication of numerous bioinspired structures. For instance, lotus-inspired topography and Salvinia-inspired structures, featuring arrays of papillae and exhibiting hydrophobicity, have been manufactured.[7,22] Moreover, springtail-skin-inspired designs have demonstrated liquid repellency in dry adhesive structures by adding the double re-entrant feature to the T-shaped fibers.[4,23]

However, the aforementioned bioinspired hydrophobic surfaces possess limited functionality due to their isotropic design. Although the fabricated hierarchical structure may exhibit properties like self-cleaning and anti-icing, directional controllability is lacking. By modifying the microstructures to incorporate an anisotropic design, programmable surface hydrophobic properties can be introduced.[24,25] The different directions of liquid movement can be granted by imitating the anisotropic texture of biological surfaces. For example, the movement of the droplets can be directed by allowing the droplets to move toward the far edge of the butterfly wing effortlessly. As the wing is tilted upward and downward, the area of the scales in contact with the droplet increases and decreases accordingly due to the compliant scales rearrangement, which results in anisotropic wettability.[1] Additionally, the droplet sits above the hierarchical surface structures to prevent water accumulation on the body. They can smoothly move along the roll-off direction and collect contaminants, reducing excess weight and enhancing the self-cleaning ability. The roll-off direction of the butterfly wing's scale horizontally orientates from its root to the tip. Each scale typically measures approximately 180 μm in length, 70 μm in width, and 3 μm in thickness.[9] Smaller features known as lamellar stacking ridges can be found on top of each scale. These lamella-stacking ridges play an integral role in influencing the hydrophobicity of the wing surface, and their dimensions are about 0.7 μm in width, 2 μm in height, and 0.22 μm in stacking spacing.[26]

In this work, inspired by the anisotropic scale design of the Morpho aega butterfly wing, artificial surfaces for directional surface wetting are fabricated via the TPP process. The interplay among TPP printing quality, architecture design, and anisotropic hydrophobic performance are investigated. Particularly, the printing process is optimized to improve the geometrical accuracy of simplified lamella-stacking ridges and the spatial arrangement of artificial wing scales. Furthermore, the hydrophobicity of the printed structures is investigated through the analysis of the contact angle of water. Moreover, anisotropic wettability is quantified by measuring the minimum required air pressure to move a water droplet under various tilting conditions ranging from 0 to 90° and in two distinct directions, namely, roll-off and roll-against directions. Surprisingly, the results reveal a reverse behavior of the artificial surfaces in contrast to their natural counterparts, possibly caused by the significant difference in equilibrium wettability between the Parylene coating and the natural butterfly wing scale surfaces. It is anticipated that the findings will facilitate the design of advanced fluid-controllable interfaces applicable in future submicroscale fluidic devices, directional coatings, and advanced engineered synthetic scaled surfaces.

2. EXPERIMENTAL SECTION

2.1. Sample Preparation and Fabrication. To prepare for the TPP process, an indium tin oxide (ITO)-coated square glass substrate (25 mm × 25 mm × 0.7 mm) is thoroughly cleaned sequentially in deionized (DI) water bath, 99.5% acetone bath, and 99.9% isopropyl alcohol (IPA) bath in a sonicator for 3, 3, and 8 min, respectively. Next, the surface of the cleaned ITO glass is activated using an oxygen plasma treatment with the Plasma Etch PE-50HF system (Plasma Etch, Caron City) for 40 s. Then, a drop of IP-S photoresist (Nanoscribe, Eggenstein-Leopoldshafen, Germany) is deposited at the center of the ITO glass, which is secured onto the substrate holder by using polyimide tape. The substrate holder is inserted into the TPP printer with the cleaned 25× objective lens installed. The 25× objective lens is positioned in contact with the photoresist to initiate polymerization of the liquid photosensitive resin using a laser beam. The fabricated microstructures are then taken out from the printer and developed in propylene glycol methyl ether acetate (PGMEA) (Merck KGaA, Darmstadt, Germany) for 20 min to dissolve any uncured excess photosensitive resin. Subsequently, the structures are bathed in IPA for 5 min to clean off any remaining PGMEA residue.

2.2. Hydrophobic Parylene Coating. Based on previously reported work, microwave-assisted chemical vapor deposition is utilized to apply a Parylene-N hydrophobic coating onto artificial butterfly scale structures and a cleaned silicon wafer. The thickness of

https://doi.org/10.1021/acsami.3c14765
ACS Appl. Mater. Interfaces 2024, 16, 9362−9370

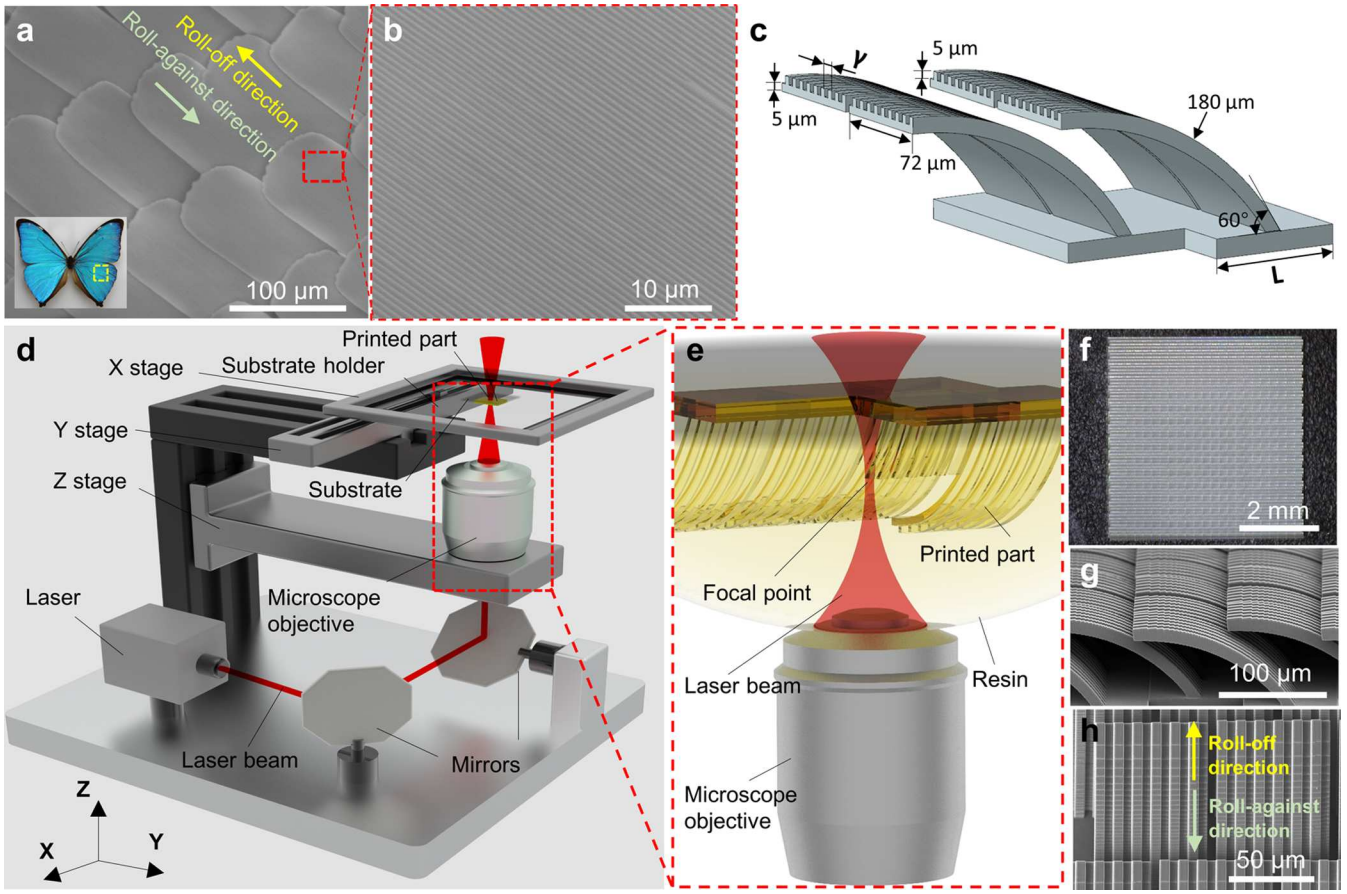

Figure 1. Design and manufacturing of bioinspired butterfly wing scales. (a) SEM image of the natural butterfly wing with roll-off and roll-against directions. (b) Zoom-in image of a scale with lamella-stacking ridges. (c) Computer-aided design model of microstructures inspired by butterfly wing's scales. (d) Schematic diagram of the TPP 3D printer. The microscope objective moves along the *z*-axis, and the substrate can move in the *xy*-plane. Two mirrors control the laser beam scanning path in the *xy*-plane. (e) Schematic diagram of the artificial butterfly scale microstructure printing process. The microscope objective is immersed in photosensitive resin, and the liquid resin at the focal point of the laser beam is polymerized. (f) Patterned artificial butterfly scales on ITO-coated glass substrate. (g, h) SEM images of the top and side views of the printed microstructures with $\gamma = 12$ μm and $L = 90$ μm.

the resulting coating is approximately 55 nm, as measured from the silicon wafer.

2.3. Scanning Electron Microscopy. The quality of the printed microstructures is inspected utilizing an FEI Quanta 650 scanning electron microscopy (SEM). To enhance imaging quality, a thin layer of gold is uniformly coated onto the samples using a 108 Manual sputter coater (Ted Pella, Redding). SEM imaging is performed in high-vacuum mode at an acceleration voltage of 10 kV to minimize the influence of atmospheric interference.

2.4. Equilibrium Contact Angle Measurement. The equilibrium contact angle measurements are carried out using a digital microscope (AF4915ZTL, Dino-Lite) with a maximum magnification of 140×. All measurements are conducted under controlled environmental conditions. For the static contact angle measurement, a 0.5 μL DI water droplet is transferred by a micropipette and dispensed onto the microstructures within the designated 5 × 5 mm^2 printed area. The contact angles are measured using ImageJ software at a view perpendicular to the artificial scales' roll-off direction.

2.5. Roll-Off and Roll-Against Pressure Measurements. A rotational stage is securely mounted vertically on a flat wall surface, and a custom-made substrate holder is attached to the rotational stage. Then, the substrate containing the printed microstructures is placed horizontally on the holder, and the roll-off direction of the microstructures is perpendicular to the rotation axis of the stage. Following that, a pneumatic nozzle, connecting to Ultimus II dispenser (Nordson EFD), is positioned perpendicularly to the edge of the printed surface with a 35 mm distance, and a 0.5 μL DI water droplet is deposited on the edge close to the pneumatic nozzle. With this setup, a stable airflow is generated via the pneumatic nozzle, and the minimum required pressure to initialize the droplet motion is measured. When the airflow direction is along the roll-off direction, the roll-off pressure (ROP) is determined when the DI water droplet shifts along the airflow direction. Likewise, roll-against pressure (RAP) is measured in the reverse roll-off direction. The experiment setup can be found in Supporting Information (Figure S1). In addition, the capability of the designed hydrophobic surface to manipulate droplets in the size range of hundreds of micrometers is demonstrated in Supporting Information (Figure S2).

3. RESULTS AND DISCUSSION

The scales on the natural wings of the Morpho aega butterfly are arranged in a radial outward orientation from the body, overlapping in a manner similar to that of roof shingles, as shown in Figure 1a. The average length and width of the butterfly wing's scale are approximately 180 and 72 μm, respectively, which aligns with values presented in another research.[9] For the designed bioinspired structure, morphologies are imitated based on natural Morph aega butterfly wing scales. The bioinspired design is a hierarchical structure that comprises a range of features organized in a structured geometrical pattern at different levels, such as curved plates on a base (level I, typical size 60−180 μm) and bent ridges on

https://doi.org/10.1021/acsami.3c14765
ACS Appl. Mater. Interfaces 2024, 16, 9362−9370

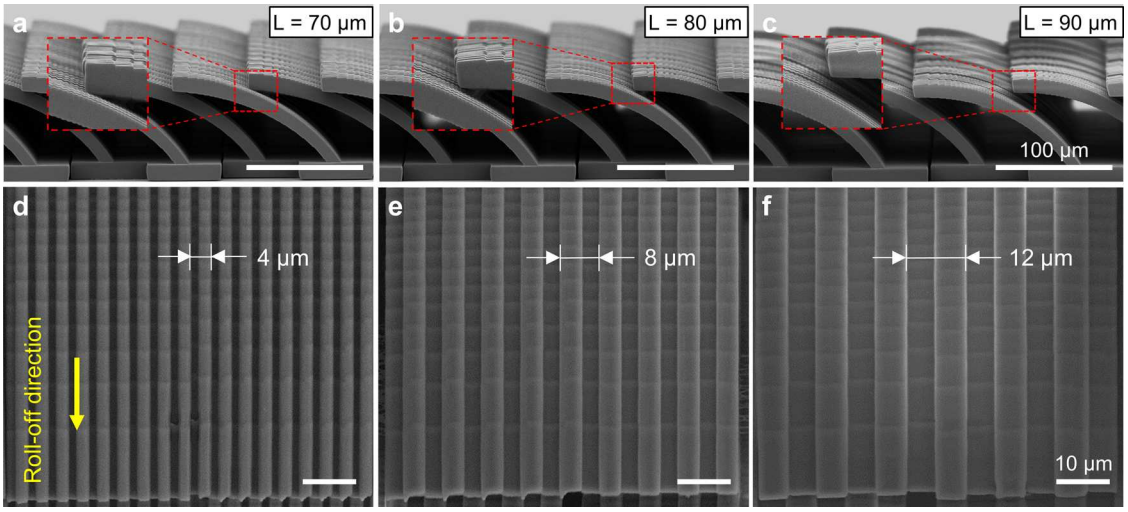

Figure 2. SEM images of TPP printed artificial scales. (a–c) Side views of the designs with γ = 6 μm, and L = 70, 80, and 90 μm. (d–f) Top view of the tip of the artificial scales with γ = 4, 8, and 12 μm.

plates (level II, 0.5–2 μm),[1,9,27,28] as shown in Figure 1a,b. The integrated structure, composed of ordered features, provides a way to manipulate the interface and dynamics of liquid–air and liquid–solid interactions, resulting in improved hydrophobicity.

At each level of the hierarchical structure, a critical dimension is identified as a variable design parameter, referred to as base length (L) and grating pitch (γ). These parameters facilitate variations in the density of curved plates per unit area (level I) and the density of ridges on a single curved plate (level II), respectively.

For Level I, the geometric design of the curved scale is inspired by the Morph aega butterfly wing scale (Figure 1c), approximately 180 μm in length and 72 μm in width. The design of 5 μm thickness and 60° inclined angle at the root of the curved plate was modified based on the reported work on synthetic butterfly wing scales.[9] The range of the base length is determined based on two factors: (1) the base length mathematically needs to have at least 70 μm to avoid intersection between adjacent scale structures; (2) observations from the natural butterfly wing reveal approximately 40% area of a scale is underneath neighboring scales, resulting in a 90 μm base length. The above dimensions of the curved plate and base provide a design close to the natural butterfly wing scale, with various artificial scale densities.

For Level II, the lamella-stacking ridges in the natural butterfly wing scale are simplified as bent ridges with a 5 μm thickness on the curved surface to facilitate fabrication (Figure 1c). Additionally, the minimum grating pitch of the ridge is restricted to 4 μm to ensure the printing quality of the fine structure. By increasing the 4 μm grating pitch to 2× and 3× larger, the 72 μm width can be evenly distributed into 18, 9, and 6 ridges.

As shown in Figure 1d, for the specific TPP printer used in imitating the scale of a butterfly wing, the Nanoscribe Photonic Professional GT2 system (Nanoscribe, Eggenstein-Leopoldshafen, Germany) employs an objective lens to fabricate microstructures. In the process, laser pulses are generated by a near-infrared laser beam in a TPP printer and used to excite the photoinitiator molecules in the photosensitive material. To ensure structural stability, the smallest feature in the design, which is the ridge structure with 2 μm width, requires at least three neighboring voxels to support the weight of a water droplet. Therefore, the 25× objective lens, capable of fabricating microstructures with a voxel size of 600 nm in diameter and 3.6 μm in height, is necessary and more suitable for efficient printing of the designed artificial scale surfaces.

The computer-aided design model of the artificial scale surface is processed by the 3D slicer DeScribe software with the default settings for the 25× objective lens using a 1 μm slicing distance and 0.5 μm hatching distance. Then, the artificial butterfly scale is printed in a bottom-up matter, starting from the scale root to the scale tip (Figure 1e). During the process, voxel fusion occurs parallel to the roll-off direction to prevent the formation of floating polymerized particles when dealing with overhanging features. To establish a robust bond between the printed structures and the substrate, the number of base layers is set to 6 with 80% laser power. The bonding strength between the ITO-coated glass and the cured IP-S resin is tested as approximately 1.1 kPa (Supporting Information, Figure S3). As a result, the anisotropic scale surface, inspired by the scales of Morpho aega butterfly wing, with 5 × 5 mm^2 is successfully fabricated on an ITO glass (Figure 1f). The artificial scales are neatly arranged with a specific offset and spacing with the same orientation as designed (Figure 1g,h).

Figure 2a–c shows the side views of the TPP fabricated microstructures inspired by the scale of a butterfly wing. It can be observed that, when the base length is set to 70 μm, the tip of the printed scales is in contact with the neighboring scales in the roll-off direction. The vertical gaps between two adjacent scales for the 80 and 90 μm base length sets are about 5 and 10 μm, respectively. As shown in Figure 2d–f, additive layers can be observed easily on top of the scales. Smoother curvature can be printed by reducing the slicing distance, but the required fabrication time increases drastically. The printed ridge structures on the artificial scales match the designed grating pitches 4, 8, and 12 μm. For all designs, the difference between the width of the peak and valley is measured to be 2 μm.

An optimized printing strategy is crucial due to the effect of microstructures' quality on hydrophobic performance.[9] The quality of the printed artificial scales can be improved by modifying the objective movement and laser scanning paths. Specifically, the objective lens moves along or against the roll-

https://doi.org/10.1021/acsami.3c14765
ACS Appl. Mater. Interfaces 2024, 16, 9362–9370

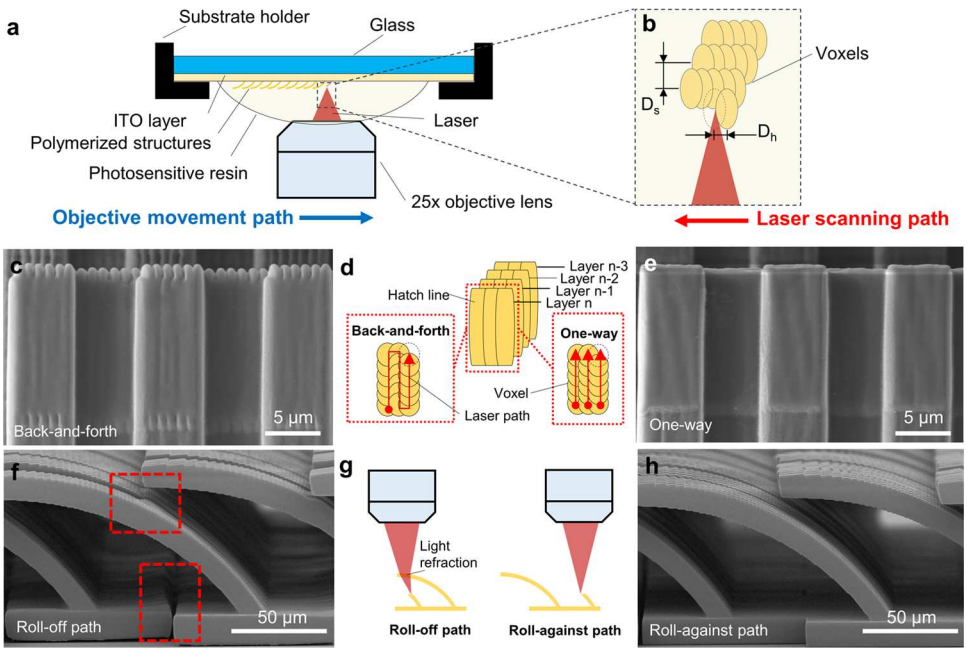

Figure 3. Influence of printing strategies on the fabrication quality of artificial scales. (a) Artificial scales are fabricated on an ITO-coated glass with a 25× objective lens moving along the roll-against direction. (b) The laser scans along the roll-off direction and the polymerized voxels are laid out with hatching (D_h) and slicing distance (D_s). (c–e) Schematic of a typical hatch line fabrication via voxel fusing with back-and-forth and one-way laser scanning paths and SEM images of the artificial scales tip with γ = 12 μm printed via the corresponding scanning paths. (f–h) Schematic of the objective moving path and the corresponding laser focal point while fabricating adjacent microstructures and SEM images of the side of the artificial scales with γ = 12 μm printed via roll-off and roll-against objective moving paths.

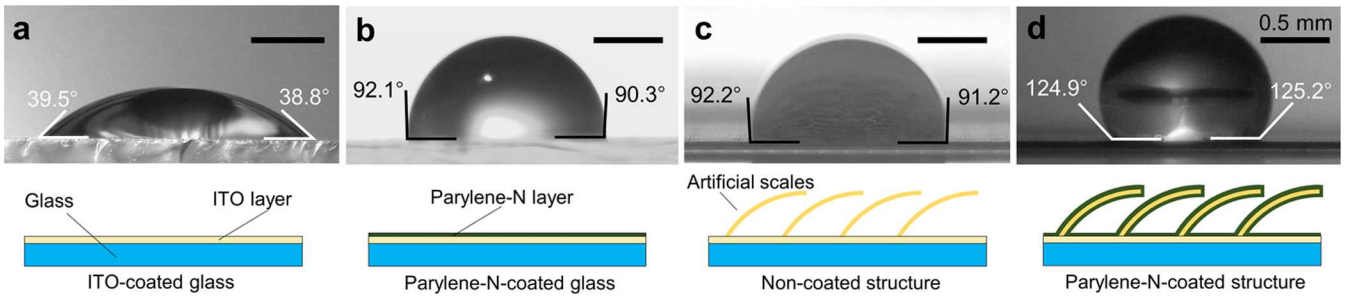

Figure 4. Equilibrium contact angle measurements for 0.5 μL water droplets. (a, b) Contact angle of water of the ITO-coated and the Parylene-N-coated glass. (c, d) Water contact angle of the noncoated and the Parylene-N-coated microstructure design with γ = 4 μm and L = 70 μm.

off direction once a row of scales is fabricated (Figure 3a). When the objective is positioned at the desired location, the laser is activated and the photoresist is polymerized with a programmed scanning path (Figure 3b). During the printing process, voxel fusion occurs along the roll-off direction to prevent the formation of floating polymerized particles when dealing with overhanging features. In addition, the optimized hatching distance D_h (0.5 μm) and slicing distances D_s (1 μm) enable fine printing quality and structural stability of high-aspect-ratio design printed in various orientations (Supporting Information, Figure S4).

As demonstrated in Figure 3c–e, two different laser scanning paths are tested, namely, back-and-forth and one-way paths. The resulting morphologies of the printed scales are shown separately in Figure 3c,e. In Figure 3c, two fused voxels are observed at the end of the hatching lines because the photopolymer resin is exposed to the laser for a longer duration when the scanning direction is reversed to print the next hatching line. On the contrary, the quality of the microstructures is improved by setting the laser scanning path to one-way, and the protuberant features are precluded, as shown in Figure 3e. However, compared with the back-and-forth laser scanning path, alternating laser scanning with a one-way path significantly increases the fabrication time due to the discontinuous printing path.

Additionally, the objective lens moving path is a factor affecting the quality of the fabricated microstructures. As shown in Figure 3f,g, the laser penetrates the completed structure if the objective lens moves along the roll-off direction when fabricating a new row of artificial scales. The printed structure underneath the adjacent fabricated scale mismatches the design due to the refraction of the laser and shifted focal point. The differences between the printed microstructures and the designs, such as detachment from the ITO glass substrate, misalignment between the base structures, and discontinuous curved surface of the artificial scale, can be precluded by moving the objective lens along the roll-against path when printing the next row of artificial scales, as shown in Figure 3h.

To demonstrate that water droplets can roll off from the surface, the printed microstructures need to have hydro-

https://doi.org/10.1021/acsami.3c14765
ACS Appl. Mater. Interfaces 2024, 16, 9362–9370

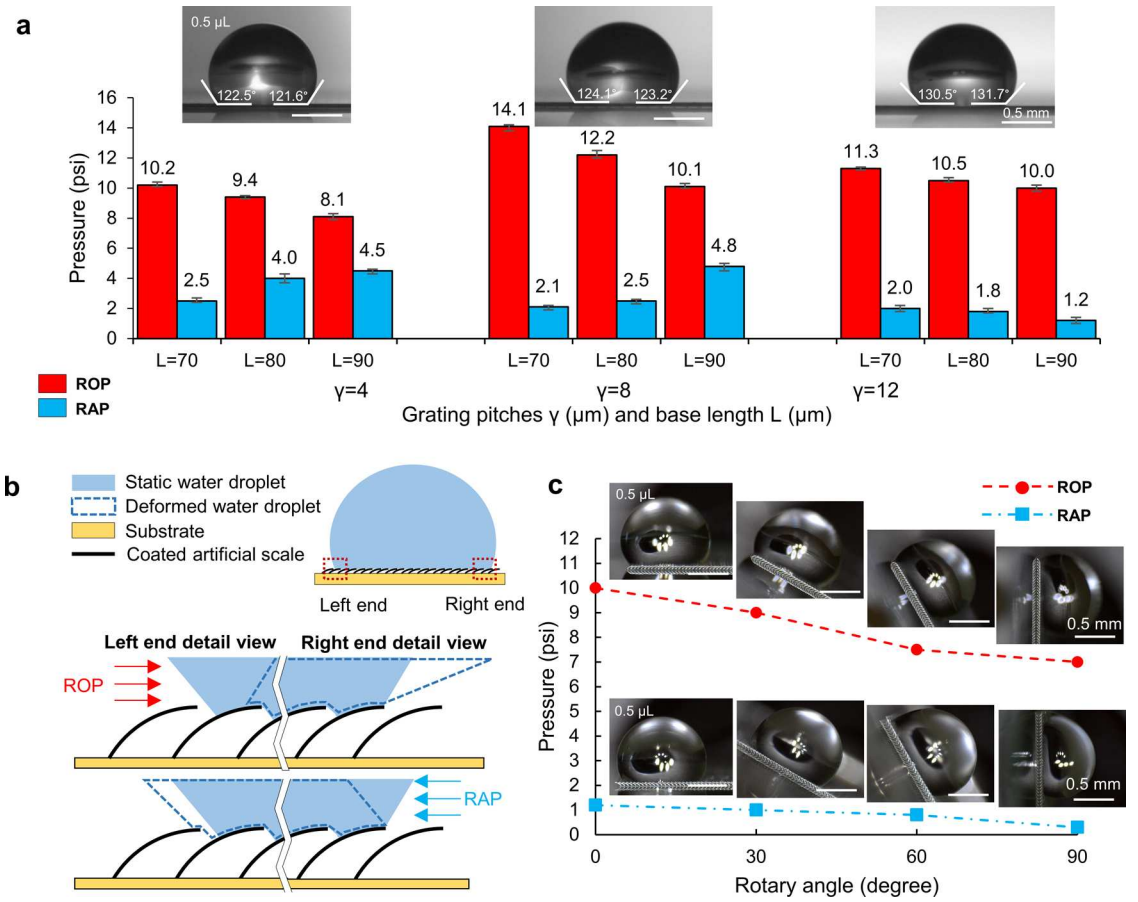

Figure 5. ROP and RAP measurements at various degrees and schematic of 0.5 μL water droplet movement under air pressure. (a) ROP and RAP for different γ and L at 0° of rotation. (b) Schematic of liquid transportation on artificial scale surface with applied air pressure. A water droplet sits on the microstructures and presents hydrophobicity in a steady state. Detailed views of the droplet's deformation under ROP and RAP at the left and right ends. (c) Average ROP and RAP for γ = 12 μm and L = 90 μm at 0, 30, 60, and 90° of rotation.

phobicity, which can be determined based on the contact angle of water. The equilibrium contact angles of water droplets on all of the surfaces with different dimensions of artificial scales are measured, as previously described. The surfaces investigated include the ITO-coated glass, Parylene-N-coated glass, as well as noncoated and Parylene-N-coated microstructures. As depicted in Figure 4a,b, the contact angles of the ITO-coated glass and the Parylene-N-coated glass are about 39 and 92°, respectively. As illustrated in Figure 4c, while the IP-S photoresist microstructures elevate the contact angle, nearing the effect seen with the Parylene-N-coated glass, they fail to realize optimal hydrophobicity. The liquid penetrates the gaps of the artificial scales, which agrees with the mechanism for surface wetting on the hierarchical structure in the Wenzel states.[29]

Consequently, an additional slender Parylene-N layer is incorporated to boost the hydrophobic attributes. Figure 4d shows that the addition of a 55 nm thick Parylene-N coating drastically increased the water to >120° for the printed artificial scales. The water droplet is supported by the air that is trapped in the gap, which matches the mechanism for surface wetting on the hierarchical structure in the Cassie–Baxter state.[29] A complete measurement of the equilibrium contact angle of water of Parylene-N-coated microstructure designs is reported in the Supporting Information (Table S1 and Figure S5). In addition, the endurance toward compression of the Parylene-N-coated artificial scale surfaces is tested to determine the maximum compressive force that the microstructure surfaces can withstand (Supporting Information, Figure S6).

To test the anisotropic properties of the fabricated surfaces, air pressure is applied to the water droplet to observe the effect of the microstructures on liquid movement in different directions. More specifically, the anisotropic behavior of the microstructures is characterized by analyzing the droplet's mobility under various tilting conditions at 0, 30, 60, and 90°. The anisotropic liquid transportability is determined through the minimum required air pressure to initiate water droplet movement in roll-off and roll-against directions, namely, ROP and RAP.

As shown in Figure 5a, the pressure required to move 0.5 μL droplets in the roll-against direction is significantly less than the roll-off direction, which is opposite to the natural butterfly wing scale. It should be noted that previous research demonstrated that the water droplet on the artificial wing scale could naturally move along the roll-off direction when the equilibrium contact angle was larger than 150°.[9] Unexpectedly, in this study, the water droplet is pinned on the surface without the assistance of airflow regardless of the variation in grating pitch and base length. A potential cause of this effect can be a lack of high enough hydrophobicity of the surfaces to let the water droplet naturally roll down.

A schematic of a droplet demonstrating the Cassie–Baxter state surface wetting is shown in Figure 5b. RAP is used to push the droplet to slide toward the scales' decline direction

https://doi.org/10.1021/acsami.3c14765
ACS Appl. Mater. Interfaces 2024, 16, 9362–9370

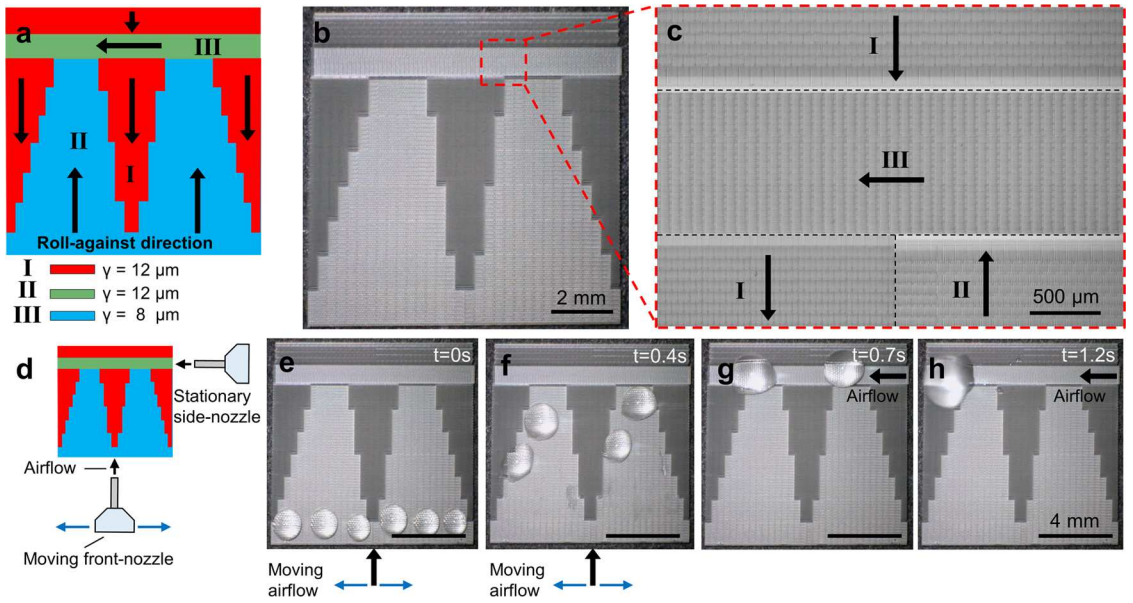

Figure 6. Demonstration of a functional hydrophobic surface for liquid transportation. (a–c) Printed microstructure surface consisting of two designs of artificial scale in three orientations. The designs with γ = 12 μm and L = 70 μm are arranged in Regions II and III, and the designs with γ = 8 μm and L = 70 μm are patterned in Region I. (d) Air pressure is provided via the pneumatic nozzles, pointing to the roll-against direction of Region II and III. (e) Six drops of DI water are deposited on the printed microstructures with an average droplet size of 1.0 μL. (f, g) Droplets are moved and merged as the airflow is applied along the roll-against direction of Region II, and Region I stops the droplets. (h) The droplets move and merge as the airflow is applied along the roll-against direction of Region III.

and make the droplet in contact with the nearby microstructures. In contrast, ROP is applied to support the droplet to move toward the scales' incline direction and cause the droplet to fall and settle onto the adjacent artificial scales, which requires more energy to exceed the hydrostatic equilibrant at the tip as well as overcome the lateral adhesion force (Supporting Information, Figure S7). As the base length increased from 70 to 80 μm, and last to 90 μm, the contact angle of water had minor changes within 1° difference, but the ROP decreased significantly. The decrease in ROP is possibly due to reducing the number of artificial scales in contact with the droplet, resulting in lower resistance in movement. Specifically, for the 4 and 8 μm grating pitch design, RAP is increased as the base length increases. This is possibly caused by the increasing gaps between the artificial scales trapping the droplet. On the contrary, for the 12 μm grating pitches design, RAP is decreased with a decrease in the base length. The higher contact angle of water presented in the 12 μm grating pitch design perhaps lowers the required energy for the droplet to slide toward the roll-off direction and jump onto the adjacent scales. In addition, ROP and RAP are decreased as the rotary angle of the stage increased because the increased gravitational potential energy along the roll-off direction reduced the need for pressure for water droplets shifting to the adjacent artificial scales, as shown in Figure 5c. Both ROP and RAP are measured for the surfaces with different printed microstructures at 0, 30, 60, and 90°; a complete measurement can be found in Supporting Information (Table S2). The anisotropic wettability is illustrated via droplets sliding off the surface along and against the roll-off direction of the printed scale under higher and lower air pressure, respectively. Such programmable wettability enables various preferred slippery directions. By patterning the artificial scales, a surface with complex anisotropic wettability can be designed and utilized in applications such as drug delivery, liquid transportation, self-cleaning, and anti-icing under pneumatic conditions.[30−32]

To explore the possibility of the proposed bioinspired microstructures for innovative water-related energy harvesting and droplet manipulating devices,[33−38] as a test case, a functional hydrophobic surface with multiple anisotropic liquid transportation directions is designed. The surface is divided into three regions with different roll-against directions (Figure 6a). The roll-against directions of Regions I, II, and III are oriented differently, and their geometrical designs (base length L and grating pitches γ) are based on the measurement of ROP and RAP. It should be noticed that all of the designs have the same base length, L = 70 μm. Specifically, Region I consists of the design with the highest ROP (γ = 8 μm), providing strong resistance to water droplet motion and limiting the droplet from rolling across the boundary when airflow is applied from the front edge and air pressure is lower than 14.1 psi. Regions II and III consist of the design with the lowest RAP (γ = 12 μm) with the same base length, avoiding undesired gaps between the three regions. This design also enables droplets to roll from the back to the front of Region II and from right to left of Region III when air pressure is higher than 2 psi. According to the aforementioned designs (γ = 8 μm and γ = 12 μm), a 1 × 1 cm^2 surface is fabricated via TPP (Figure 6b,c).

To further demonstrate the anisotropic hydrophobicity behaviors, the water droplets, on top of the horizontally placed fabricated artificial surface, are tested under airflow generated by two pneumatic nozzles. Specifically, two nozzles are separately positioned 35 mm from the front and right edges of the fabricated surface. To minimize the residue on the designed surface, possibly due to fast droplet sliding (as shown in Supporting Information, Figure S8), a consistent 5 psi air pressure was provided via the pneumatic nozzles, pointing to the roll-against direction of Region II and III (Figure 6d). In addition, to push all of the water droplets distributed along the

https://doi.org/10.1021/acsami.3c14765
ACS Appl. Mater. Interfaces 2024, 16, 9362−9370

front edge of the printed surface, the front nozzle moves perpendicular to the roll-against direction of Region II and remains the 35 mm distance for the fabricated surface.

In this study, to investigate the behavior of anisotropic transportability of the proposed design, six droplets are initially deposited on left and right segments ("3 + 3") in Region II (Figure 6e). Under external airflow, we noticed that the deposited water droplets are moved and accumulated together as the width of Region II decreases (Figure 6f). Subsequently, the majority portion of the accumulated droplet moves within Region II along its roll-against direction. The remaining portion of the water droplets pinned by the microstructures in Region I is dragged by the water surface tension and moves along the boundary of Region II. Afterward, the motion of the accumulated droplet is pinned on Region III due to the designed roll-against direction (Figure 6g). Finally, the pinned water droplets are moved by the stationary airflow generated by the side nozzle and removed from the fabricated surface (Figure 6h).

According to the observation, the synthetic bioinspired hydrophobic surface demonstrates the capability of transporting water droplets along the roll-against direction by pinning droplets in undesired regions until supplied airflow aligns with favorable regions. In addition, the "1 + 1" and "2 + 2" droplet patterns are also tested under the same conditions, and the results are included in the Supporting Information (Figures S9 and S10). From these findings, effective controllable fluid transportation can be achieved by fabricating engineered hydrophobic surfaces using multiple designs based on the Morph aega butterfly scale via TPP. Such engineered structures coupled with advanced AM can facilitate the implementation of applications, such as energy harvesting and droplet manipulating devices.

4. CONCLUSIONS

In this paper, inspired by scales of butterfly wings, various 3D hydrophobic microstructure surfaces are fabricated on ITO-coated glass slides using the TPP technique. The quality of the artificial butterfly scale is improved by implementing a one-way laser scanning strategy and making adjustments to the objective lens movement in alignment with the roll-against direction during printing. The fabricated microstructures enhance the hydrophobicity of the surfaces and significantly increase the contact angle of water when coated with a thin layer of Parylene-N. The hydrophobicity is further improved by increasing the grating pitch length of the ridge structure on artificial scales. With the hydrophobic coating, anisotropic wettability is presented on the engineered 3D structured surface, which showcases less favor to move along the roll-off direction than along the roll-against direction, opposite the natural counterparts. In terms of the geometrical parameters, the increase in the base length of the printed scales improves the movability of the droplet. Still, it encounters more difficulty in moving along the roll-against direction due to reduced hydrophobicity. The presented TPP printed scale surfaces with directional wettability hold potential for various applications, such as tunable fluid transport surfaces, self-cleaning exteriors, and microchannel filling. Future work may include modeling the droplet movement on the artificial scale to determine the optimal dimensions for reducing resistance in the roll-against direction.

ASSOCIATED CONTENT

Supporting Information

The Supporting Information is available free of charge at https://pubs.acs.org/doi/10.1021/acsami.3c14765.

Experimental setup for roll-off and roll-against pressures measurement; investigation of controlling smaller droplets; bonding strength between the printed microstructures and the substrate; TPP fabricated high-aspect-ratio structure in various orientations with fine printing quality; contact angle of water on Parylene-N-coated microstructure designs; mechanical breakdown strength of the printed microstructures; explanation of the anisotropic phenomenon; droplets residue investigation; "1 + 1" and "2 + 2" droplet patterns tested on functional hydrophobic surface; contact angles of water measurements; and measurement of ROP and RAP of Parylene-N-coated microstructures (PDF)

AUTHOR INFORMATION

Corresponding Authors

Meng Cheng − *Key Laboratory of Metallurgical Equipment and Control Technology, Ministry of Education, Wuhan University of Science and Technology, Wuhan, Hubei 430081, China*; Email: chengmeng@wust.edu.cn

Daewon Kim − *Department of Aerospace Engineering, Embry-Riddle Aeronautical University, Daytona Beach, Florida 32114, United States*; Email: daewon.kim@erau.edu

Yizhou Jiang − *Department of Aerospace Engineering, Embry-Riddle Aeronautical University, Daytona Beach, Florida 32114, United States*; orcid.org/0009-0009-4802-8217; Email: yizhou.jiang@erau.edu

Authors

Zefu Ren − *Department of Aerospace Engineering, Embry-Riddle Aeronautical University, Daytona Beach, Florida 32114, United States*

Zhuoyuan Yang − *Department of Aerospace Engineering, Embry-Riddle Aeronautical University, Daytona Beach, Florida 32114, United States*

Rishikesh Srinivasaraghavan Govindarajan − *Department of Aerospace Engineering, Embry-Riddle Aeronautical University, Daytona Beach, Florida 32114, United States*

Foram Madiyar − *Department of Physical Science, Embry-Riddle Aeronautical University, Daytona Beach, Florida 32114, United States*

Complete contact information is available at: https://pubs.acs.org/10.1021/acsami.3c14765

Author Contributions

‖Z.R. and Z.Y. contributed equally to this work. The manuscript was written through contributions from all authors. All authors have approved the final version of the manuscript.

Notes

The authors declare no competing financial interest.

ACKNOWLEDGMENTS

This material is based upon work supported partially by the National Science Foundation under grant nos. 2018853 and 2050887 and the National Natural Science Foundation of China under grant no. 52201272. The opinions, findings, and conclusions or recommendations expressed are those of the authors and do not necessarily reflect the views of the National

Science Foundation and the National Natural Science Foundation of China.

REFERENCES

(1) Zheng, Y.; Gao, X.; Jiang, L. Directional Adhesion of Superhydrophobic Butterfly Wings. *Soft Matter* **2007**, *3* (2), 178−182.
(2) Lv, J.; Song, Y.; Jiang, L.; Wang, J. Bio-Inspired Strategies for Anti-Icing. *ACS Nano* **2014**, *8* (4), 3152−3169.
(3) Plamadeala, C.; Gosain, S. R.; Hischen, F.; Buchroithner, B.; Puthukodan, S.; Jacak, J.; Bocchino, A.; Whelan, D.; O'Mahony, C.; Baumgartner, W.; Heitz, J. Bio-Inspired Microneedle Design for Efficient Drug/Vaccine Coating. *Biomed. Microdevices* **2020**, *22* (1), No. 8.
(4) Dayan, C. B.; Chun, S.; Krishna-Subbaiah, N.; Drotlef, D.-M.; Akolpoglu, M. B.; Sitti, M. 3D Printing of Elastomeric Bioinspired Complex Adhesive Microstructures. *Adv. Mater.* **2021**, *33* (40), No. 2103826.
(5) Yang, L.; Shen, X.; Yang, Q.; Liu, J.; Wu, W.; Li, D.; Du, J.; Zhang, B.; Fan, S. Fabrication of Biomimetic Anisotropic Super-Hydrophobic Surface with Rice Leaf-Like Structures by Femtosecond Laser. *Opt. Mater.* **2021**, *112*, No. 110740.
(6) Wang, Y.; Shang, L.; Chen, G.; Sun, L.; Zhang, X.; Zhao, Y. Bioinspired Structural Color Patch with Anisotropic Surface Adhesion. *Sci. Adv.* **2020**, *6* (4), No. eaax8258.
(7) Lantada, A. D.; Hengsbach, S.; Bade, K. Lotus-on-Chip: Computer-Aided Design and 3D Direct Laser Writing of Bioinspired Surfaces for Controlling the Wettability of Materials and Devices. *Bioinspiration Biomimetics* **2017**, *12* (6), No. 066004.
(8) Tellechea-Robles, L. E.; Méndez-Alonzo, R.; Molina-Freaner, F. E.; Maldonado, A. Microstructure and Hydrophobicity of the External Surface of a Sonoran Desert Beetle. *Biomimetics* **2022**, *7* (2), No. 38.
(9) Zhao, H.; Park, S. J.; Solomon, B. R.; Kim, S.; Soto, D.; Paxson, A. T.; Varanasi, K. K.; Hart, A. J. Synthetic Butterfly Scale Surfaces with Compliance-Tailored Anisotropic Drop Adhesion. *Adv. Mater.* **2019**, *31* (14), No. 1807686.
(10) Yoon, Y.; Kim, D.; Lee, J.-B. Hierarchical Micro/Nano Structures for Super-Hydrophobic Surfaces and Super-Lyophobic Surface Against Liquid Metal. *Micro Nano Syst. Lett.* **2014**, *2* (1), No. 3.
(11) Xu, Y.; Mao, H.; Liu, C.; Du, Z.; Yan, W.; Yang, Z.; Partanen, J.; Chen, Y. Hopping Light Vat Photopolymerization for Multiscale Fabrication. *Small* **2023**, *19* (11), No. 2205784.
(12) Joyee, E. B.; Pan, Y. Multi-Material Additive Manufacturing of Functional Soft Robot. *Procedia Manuf.* **2019**, *34*, 566−573.
(13) Khan, S.; Joshi, K.; Deshmukh, S. A Comprehensive Review on Effect of Printing Parameters on Mechanical Properties of FDM Printed Parts. *Mater. Today: Proc.* **2022**, *50*, 2119−2127.
(14) Xing, R.; Yang, B.; Huang, R.; Qi, W.; Su, R.; Binks, B. P.; He, Z. Three-Dimensionally Printed Bioinspired Superhydrophobic Packings for Oil-in-Water Emulsion Separation. *Langmuir* **2019**, *35* (39), 12799−12806.
(15) Gu, D.; Shi, X.; Poprawe, R.; Bourell, D. L.; Setchi, R.; Zhu, J. Material-Structure-Performance Integrated Laser-Metal Additive Manufacturing. *Science* **2021**, *372* (6545), No. eabg1487.
(16) Yang, J.; Gu, D.; Lin, K.; Zhang, Y.; Guo, M.; Yuan, L.; Zhang, H.; Zhang, H. Laser Additive Manufacturing of Bio-Inspired Metallic Structures. *Chin. J. Mech. Eng.: Addit. Manuf. Front.* **2022**, *1* (1), No. 100013.
(17) Mekhiel, S.; Koshy, P.; Elbestawi, M. A. Additive Texturing of Metallic Surfaces for Wetting Control. *Addit. Manuf.* **2021**, *37*, No. 101631.
(18) Li, H.; Dai, J.; Wang, Z.; Zheng, H.; Li, W.; Wang, M.; Cheng, F. Digital Light Processing (DLP)-Based (Bio)Printing Strategies for Tissue Modeling and Regeneration. *Aggregate* **2023**, *4* (2), No. e270.
(19) Davoudinejad, A.; Ribo, M. M.; Pedersen, D. B.; Islam, A.; Tosello, G. Direct Fabrication of Bio-Inspired Gecko-Like Geometries with Vat Polymerization Additive Manufacturing Method. *J. Micromech. Microeng.* **2018**, *28* (8), No. 085009.
(20) Lin, Y.; Zhou, R.; Xu, J. Superhydrophobic Surfaces Based on Fractal and Hierarchical Microstructures Using Two-Photon Polymerization: Toward Flexible Superhydrophobic Films. *Adv. Mater. Interfaces* **2018**, *5* (21), No. 1801126.
(21) Raimondi, M. T.; Eaton, S. M.; Nava, M. M.; Laganà, M.; Cerullo, G.; Osellame, R. Two-Photon Laser Polymerization: from Fundamentals to Biomedical Application in Tissue Engineering and Regenerative Medicine. *J. Appl. Biomater. Funct. Mater.* **2012**, *10* (1), 56−66.
(22) Tricinci, O.; Pignatelli, F.; Mattoli, V. 3D Micropatterned Functional Surface Inspired by Salvinia Molesta via Direct Laser Lithography for Air Retention and Drag Reduction. *Adv. Funct. Mater.* **2023**, *33*, No. 2206946.
(23) Yamaguchi, M. Microfabrication of Re-entrant Surface with Hydrophobicity/Oleophobicity for Liquid Foods. *Sci. Rep.* **2020**, *10* (1), No. 2250.
(24) Xu, J.; Xiu, S.; Lian, Z.; Yu, H.; Cao, J. Bioinspired Materials for Droplet Manipulation: Principles, Methods and Applications. *Droplet* **2022**, *1* (1), 11−37.
(25) Leng, X.; Sun, L.; Long, Y.; Lu, Y. Bioinspired Superwetting Materials for Water Manipulation. *Droplet* **2022**, *1* (2), 139−169.
(26) Watanabe, K.; Hoshino, T.; Kanda, K.; Haruyama, Y.; Kaito, T.; Matsui, S. Optical Measurement and Fabrication from a Morpho-Butterfly-Scale Quasistructure by Focused Ion Beam Chemical Vapor Deposition. *J. Vac. Sci. Technol., B: Microelectron. Nanometer Struct.–Process., Meas., Phenom.* **2005**, *23* (2), 570−574.
(27) Chen, Z.; Zhang, Z.; Wang, Y.; Xu, D.; Zhao, Y. Butterfly Inspired Functional Materials. *Mater. Sci. Eng., R* **2021**, *144*, No. 100605.
(28) Liu, X.; Zhang, S.; Zhang, H. Microstructure of Butterfly Wing Scale and Simulation of Structural Solor. *Optik* **2016**, *127* (4), 1729−1733.
(29) Hejazi, V.; Moghadam, A. D.; Rohatgi, P.; Nosonovsky, M. Beyond Wenzel and Cassie−Baxter: Second-Order Effects on the Wetting of Rough Surfaces. *Langmuir* **2014**, *30* (31), 9423−9429.
(30) Zhan, Y.; Ruan, M.; Li, W.; Li, H.; Hu, L.; Ma, F.; Yu, Z.; Feng, W. Fabrication of Anisotropic PTFE Superhydrophobic Surfaces Using Laser Microprocessing and Their Self-Cleaning and Anti-Icing Behavior. *Colloids Surf., A* **2017**, *535*, 8−15.
(31) Wang, C.; Ding, K.; Song, Y.; Jia, X.; Lin, N.; Duan, Ja. Femtosecond Laser Patterned Superhydrophobic Surface with Anisotropic Sliding for Ddroplet Manipulation. *Opt. Laser Technol.* **2024**, *168*, No. 109829.
(32) Zhang, Q.; Bai, X.; Li, Y.; Zhang, X.; Tian, D.; Jiang, L. Ultrastable Super-Hydrophobic Surface with an Ordered Scaly Structure for Decompression and Guiding Liquid Manipulation. *ACS Nano* **2022**, *16* (10), 16843−16852.
(33) Lin, Z.-H.; Cheng, G.; Lee, S.; Pradel, K. C.; Wang, Z. L. Harvesting Water Drop Energy by a Sequential Contact-Electrification and Electrostatic-Induction Process. *Adv. Mater.* **2014**, *26* (27), 4690−4696.
(34) Tang, X.; Zhu, P.; Tian, Y.; Zhou, X.; Kong, T.; Wang, L. Mechano-Regulated Surface for Manipulating Liquid Droplets. *Nat. Commun.* **2017**, *8* (1), No. 14831.
(35) Wang, J.; Gao, W.; Zhang, H.; Zou, M.; Chen, Y.; Zhao, Y. Programmable Wettability on Photocontrolled Graphene Film. *Sci. Adv.* **2018**, *4* (9), No. eaat7392.
(36) Wang, J.; Sun, L.; Zou, M.; Gao, W.; Liu, C.; Shang, L.; Gu, Z.; Zhao, Y. Bioinspired Shape-Memory Graphene Film with Tunable Wettability. *Sci. Adv.* **2017**, *3* (6), No. e1700004.
(37) Zhang, X.; Sun, L.; Wang, Y.; Bian, F.; Wang, Y.; Zhao, Y. Multibioinspired Slippery Surfaces with Wettable Bump Arrays for Droplets Pumping. *Proc. Natl. Acad. Sci. U.S.A.* **2019**, *116* (42), 20863−20868.
(38) Ben, S.; Zhou, T.; Ma, H.; Yao, J.; Ning, Y.; Tian, D.; Liu, K.; Jiang, L. Multifunctional Magnetocontrollable Superwettable-Microcilia Surface for Directional Droplet Manipulation. *Adv. Sci.* **2019**, *6* (17), No. 1900834.

https://doi.org/10.1021/acsami.3c14765
ACS Appl. Mater. Interfaces 2024, 16, 9362−9370